ACS OMEGA

Article

Cite This: ACS Omega 2019, 4, 22497−22503

http://pubs.acs.org/journal/acsodf

Inkjet-Printed Imbedded Graphene Nanoplatelet/Zinc Oxide Bulk Heterojunctions Nanocomposite Films for Ultraviolet Photodetection

Brent Cook,*,† Maogang Gong,† Alex Corbin,§ Dan Ewing,‡ Ashley Tramble,‡ and Judy Wu*,†

†Department of Physics and Astronomy, University of Kansas, Lawrence, Kansas 66045, United States

‡Department of Energy's National Security Campus, Kansas City, Missouri 64147, United States

§Shawnee Mission East High School, 7500 Mission Road, Prairie Village, Kansas 66208, United States

Supporting Information

ABSTRACT: A ZnO sol−gel precursor (ZnOPr) and graphene nanoplatelets (GnPs) are mixed into a composite ink for inkjet printing photodetectors with bulk heterojunctions of ZnO/GnP on a heated SiO_2/Si substrate. Heating of the SiO_2/Si wafers at ∼50 °C was found optimal to prevent segregated droplets on the hydrophobic surface of the SiO_2/Si substrate during printing. After printing the ZnO/GnP channels, thermal annealing at 350 °C for 2 h was performed for crystallization of ZnO and formation of the ZnO/GnP heterojunctions. The GnP concentration was varied from 0, 5, 20, and 30 mM to evaluate optimal formation of the ZnO/GnP bulk heterojunction nanocomposites based on ultraviolet photoresponse performance. The best performance was observed at the 20 mM GnP concentration with the photoresponsivity reaching 2.2 A/W at an incident ultraviolet power of 2.2 μW and a 5 V bias. This photoresponsivity is an order of magnitude better than the previously reported counterparts, including 0.13 mA/W for dropcasted ZnO-graphite composites and much higher than 0.5 A/W for aerosol printed ZnO. The improved performance is attributed to the ZnO/GnP bulk heterojunctions with improved interfaces that enable efficient exciton dissociation and the charge transport. The developed inkjet printing of sol−gel composite inks approach can be scalable and low cost for practical applications.

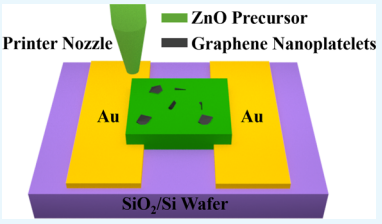

INTRODUCTION

Zinc oxide (ZnO) and graphene, especially their nanohybrids, have been extensively studied for a wide variety of applications ranging from photodetectors,[1−11] gas sensors,[12,13] and stress/strain sensors.[10,14−16] The appeal of ZnO and graphene for these applications is that ZnO is a wide direct bandgap (3.4 eV) material, piezoelectric, biocompatible, and inexpensive, while graphene has high charge mobility, transparent, environmentally stable, and chemically inert.[17−20] Nanohybrids of ZnO and graphene are typically fabricated by predepositing graphene first via chemical vapor deposition (CVD) and then incorporating the ZnO on the top through hydrothermal growth,[21,22] sputtering,[8] atomic layer deposition (ALD),[23] spin-coating sol−gel precursors,[3] electrochemical deposition,[24] vapor transport,[20] and dropcasting prefabricated ZnO nanostructures.[4] However, synthesis methods such as CVD require high temperatures and a controlled gaseous environment and other methods such as sputtering and ALD require expensive high-vacuum systems.[8,19,23] In addition, these methods deposit a film everywhere and require additional steps of advanced lithography to define the active channels for devices.

Inkjet printing provides a unique approach to deposit functional materials directly to a select region without a direct contact with the substrate. In particular, inkjet printing of nanocomposites of ZnO and graphite nanocomposites is appealing for flexible photodetectors[25] and stress/strain sensors.[26] Compared to other inkjet-printed ZnO devices, which commonly have photoresponsivity on an order of ∼10^{-3} A/W,[25,27,28] the inkjet-printed ZnO/graphene nanocomposites, such as composites consisting of presynthesized ZnO mixed with graphene flakes, have enhanced photoresponsivity on an order of ∼10^{-2} A/W and rise and fall times of ∼0.1 s.[4,29,30] The ZnO/graphene composite devices can have above two orders of magnitude improvement in photoresponsivity; however, they still lack a poor interface between prefabricated ZnO and graphene structures.[4,13,27] One way to resolve this issue is to use a nanocomposite ink by mixing a ZnO precursor and graphene nanoplatelets to allow a clean ZnO/graphene interface to form during the ZnO crystallization while graphene is maintained intact. To do this, the challenges in inkjet printing due to the effect of the substrate surface hydrophobicity and ink fluidity on the morphology of the printed films must be addressed. For example, in recent works by our group, heat-assisted printing was explored on the hydrophobicity of SiO_2. It has been found that the formation of large droplets can be suppressed with moderate heating of the substrates to ∼50 °C for printing while also keeping the

Received: September 26, 2019
Accepted: December 5, 2019
Published: December 18, 2019

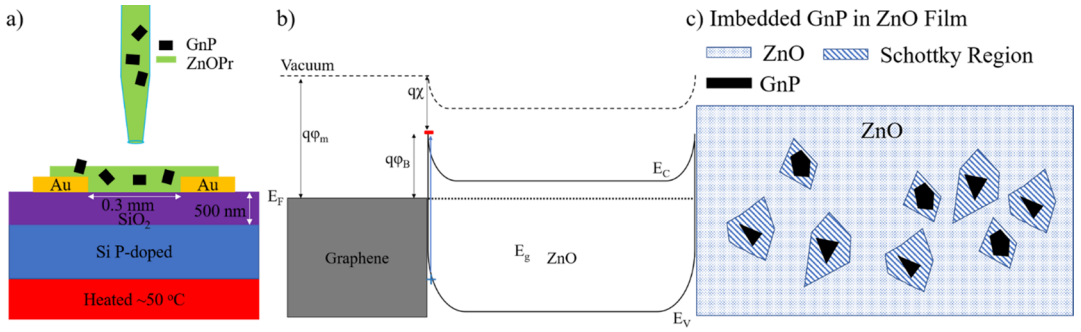

Figure 1. (a) Printing of ZnO precursor (ZnOPr)/graphene nanoplatelet composite ink, (b) energy band diagram of graphene and ZnO Schottky interface, and (c) a schematic of graphene nanoplatelets with the Schottky interface.

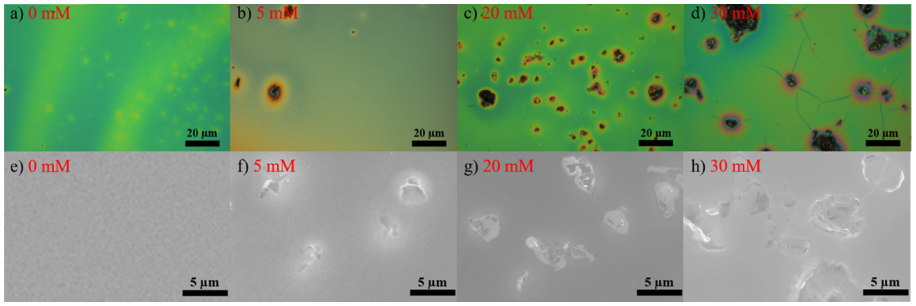

Figure 2. Optical images are depicted for (a) 0 mM, (b) 5 mM, (c) 20 mM, and (d) 30 mM GnP in ZnO/GnP nanocomposite films and (e–h) the respective SEM images.

nozzle near the surface to form a liquid bridge for capillary action-assisted printing to avoid spraying that is prevalent in printing highly fluid inks.[31,32] In addition, the composite ink has to satisfy specific requirements to be considered printable. These requirements are known as the Reynolds, Weber, and Ohnesorge numbers, which are defined as the following $N_R = v\rho a/\eta$, $N_W = \rho a v^2/\gamma$, and $N_O = (N_W)^{1/2}/N_R = \eta/(\gamma\rho a)^{1/2}$, where γ, η, ρ, a, and v are the surface tension, dynamic velocity, drop diameter, and velocity, respectively.[33,34] Together, these numbers give rise to the "Z" parameter, which is defined as the inverse Ohnesorge number, $Z = 1/N_O$, and should be in a range of 1–10 for printability, too small or too large of a Z value will give a very viscous or too fluid ink, respectively.[33,34] This indicates the importance in controlling the ink fluidity characteristic for printability, especially for nanocomposite inks.

In this work, graphene nanoplatelets (GnP) were incorporated in a ZnO precursor (ZnOPr) solution to make a nanocomposite ink (ZnOPrGnP) for printing ultraviolet (UV) photodetectors consisting of a network of bulk heterojunctions of ZnO/GnP formed during post crystallization of ZnO. The GnP concentration was varied from 0 to 30 mM in the ZnO precursor to define an optimal ink for inkjet printing of a ZnO/GnP network structure for photodetection. At an optimal GnP concentration of 20 mM, the UV photoresponsivity reached up to 2.2 A/W and the on/off ratio reached up to 10^2–$10.^3$ This is four orders of magnitude higher in photoresponsivity than the previously reported inkjet-printed ZnO/graphene nanocomposite UV photodetectors[4] and one order of magnitude larger than an inkjet-printed flexible ZnO UV photoconductor.[27] This improved responsivity can be ascribed to the introduction of the ZnO/GnP heterojunctions for more efficient exciton dissociation and charge transfer at the ZnO/GnP interface.

RESULTS AND DISCUSSION

Figure 1a illustrates schematically the inkjet printing of the ZnOPrGnP nanocomposite ink onto the SiO_2/Si channel between two Au electrodes at a substrate temperature of 50 °C. With assistance of the piezoelectric vibration in the boron/silicate glass nozzle, the ZnOPrGnP nanocomposite ink was dispersed from the nozzle to form a ZnOPrGnP precursor film. Afterward, the annealing was performed to convert the ZnO precursor to the polycrystalline ZnO/GnP composite film. It should be noted that GnPs remain intact during the ZnO annealing process, which is consistent to our previous works using graphene made in chemical vapor deposition.[3,21] By keeping GnPs intact during the annealing, the embedded GnPs can form Schottky junctions with crystalline ZnO at the ZnO/GnP interface.[6,7,9,10,19] Specifically, the Schottky junction at the ZnO/GnP interface is formed due to the charge transfer from ZnO to graphene, which is induced by the energy work function offset of ZnO ($q\chi$ = 4.4 eV) and graphene ($q\varphi_m$ = 4.6 eV).[35] As a result, the Fermi energy of the graphene (ZnO) is increased (decreased), resulting in band bending near the interface and an energy barrier ($q\varphi_B$ = 0.2 eV) formation between the graphene and ZnO (Figure 1b).[35] Alternatively, this same mechanism can also be used as a method for trapping charges on the ZnO/GnP Schottky interface, which can reduce charge carrier concentration in ZnO as shown in Figure 1c. This gives the ZnO/GnP nanocomposites several advantages over the ZnO only photoconductive photodetectors.[25,27] First, the dark current of the device is greatly reduced by introduction of the Schottky junctions created at the graphene ZnO/GnP interfaces. In addition, the ZnO/GnP Schottky junctions can facilitate exciton dissociation into free electrons and holes and therefore increase the photocurrent I_{ph}. Finally, the effective electron–hole recombination will be reduced in the nanocomposite devices due to the more effective charge

DOI: 10.1021/acsomega.9b03173
ACS Omega 2019, 4, 22497–22503

transport from well-distributed Schottky junctions throughout the nanocomposite to electrodes. Last, the efficiency of exciton dissociation and the follow-up charge transfer would rely on the concentration of the ZnO/GnP heterojunctions based on the minority diffusion length in the nanocomposite, which in turn determines the photoresponsivity of the device in a similar way to bulk heterojunction photovoltaics.[36] Under ultraviolet irradiation above the cutoff of a ZnO energy bandgap of 3.4 eV, an electron−hole pair is created (Figure 1b) and the electron and holes are drawn away from one another due to the band bending at the interface with the holes (electrons) moving to higher energy (lower energy) in the valence band (conduction band).

Figure 2a,b,c,d exhibits the optical images of the printed ZnO/GnP samples with GnP concentrations of 0, 5, 20, and 30 mM, respectively. With increasing GnP concentrations, features appear in the printed nanocomposite films and the dimension of the features increases as well primarily due to clumping of GnPs at higher concentrations. It should be pointed out that the clumping of GnPs is unfavorable since it will reduce the number of the Schottky junctions due to reduced ZnO/GnP interface area and the performance of the optoelectronic devices based on the ZnO/GnP nanocomposites. Figure 2e,f,g,h includes SEM images taken on the same set of samples shown in Figure 2a,b,c,d, respectively. At 5 mM GnP concentration, the features on the printed ZnO/GnP nanocomposite film have the dimension of approximately 3−4 μm. The feature size remains approximately the same, with a few larger ones of 5−7 μm on the sample with 20 mM GnP. At 30 mM GnP concentration, the features become significantly larger to about 6−12 μm in lateral dimension, indicating clumping of the GnP flakes becomes serious at 30 mM or concentrations.

The Raman spectrum on a representative ZnO/GnP nanocomposite film of 20 mM GnP concentration is shown in Figure 3a, graphene is known to have two peaks, the G peak

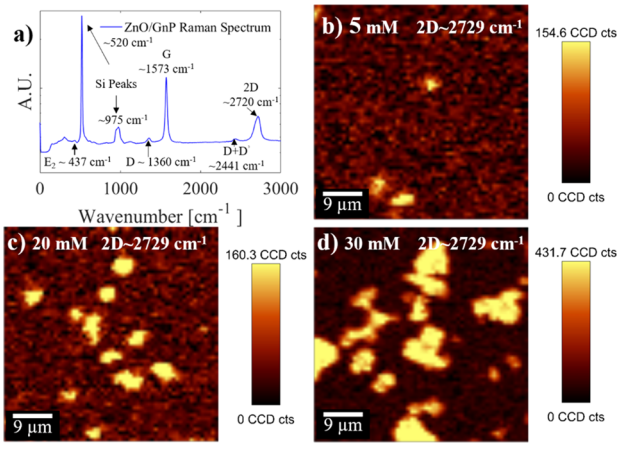

Figure 3. (a) Raman spectrum of the 20 mM ZnO/GnP film and (b−d) Raman maps of graphene 2D peak for GnP/ZnO nanocomposite samples of 5, 20, and 30 mM GnP concentrations.

at approximately 1584 cm^{-1} and the 2D peak at 2729 cm^{-1}, and a 2D/G peak ratio greater than 1.5 indicates single layer; otherwise, it is assumed to be multilayer graphene.[37−39] It should be noted that the difference in the Raman spectra of the ZnO/GnP nanocomposite films with the GnP concentration varied in the range of this experiment is negligible as the relative peaks all showed similar traits (Figures S1). The shifts in the 2D peak and G peak away from single layer graphene are consistent with multilayer graphene and graphite nanoplatelets.[37,38] In addition, there is a peak at 436 cm^{-1} called the E_2 peak, which is associated with the c axis of the sol−gel-grown ZnO wurzite structure being perpendicular to the substrate.[40] The other peaks in Figure 3a are associated with the Si/SiO_2 wafer and the most intensive one is the peak at 520 cm^{-1}. From the Raman map in Figure 3b,c,d, we can see that the flake sizes for the GnPs are approximately 2−4, 5−8, and 8−12 μm, which can be observed for the 5, 20, and 30 mM GnP concentrations, respectively, which are consistent with the SEM images. Specifically, the areal density of the features is 10^3 flakes/mm^2 at 5 mM GnP, which increased to 10^4 flakes/mm^2 at 20 mM GnP. While the density at 30 mM does not increase proportionally with the GnP concentration, the dimension of the features is 10.2 ± 1.9 μm, while at 20 mM, the dimension of features is 5.4 ± 1.0 that is two times different in average size and variation, indicating an increase in segregation of the GnPs to GnP clumps in the ZnO/GnP nanocomposites at 30 mM.

The photocurrent as a function of the bias voltage is shown in Figure 4a, where the photocurrent is defined as $I_{ph} = I_{UV} -$

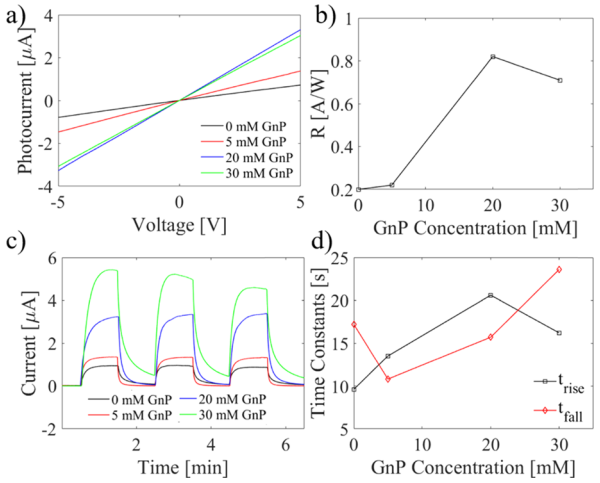

Figure 4. (a) Photocurrent as a function of the bias voltage and (b) responsivity measured on ZnO/GnP nanocomposited films with 0, 5, 20, and 30 mM GnP concentrations. (c) Dynamic UV photoresponse (340 nm) at a 5 V bias of the same four samples in (a) and (d) the extracted rise and fall times from (c) for the four samples.

I_{Dark}, where I_{UV} and I_{Dark} are the currents of the device under UV illumination and no illumination, respectively, with the UV light source being 340 nm in wavelength at a power of P = 4.6 ± 0.3 μW. In the photocurrent−voltage characteristic curves, the photocurrent increases monotonically with the GnP concentration up to 20 mM, confirming the benefits of the ZnO/GnP Schottky junctions for efficient exciton dissociation and charge transfer. At a higher GnP concentration of 30 mM, this benefit is reduced due to the GnP clumping. This trend can be seen clearly in the photoresponsivity as a function of GnP concentration in Figure 4b, where the photoresponsivity R is defined as $R = I_{ph}/P$.[41] The photoresponsivity was measured with a 5 V bias at a wavelength of 340 nm and power of P = 4.6 ± 0.3 μW. Specifically, the photoresponsivity increases from 0.20 A/W for the printed ZnO only device to 0.22 A/W for the 5 mM ZnO/GnP sample and to 0.82 A/W

DOI: 10.1021/acsomega.9b03173
ACS Omega 2019, 4, 22497−22503

for 20 mM ZnO/GnP. At a higher GnP concentration of 30 mM, it decreases to 0.71 A/W. In addition, the photoresponsivity as a function of voltage was also calculated and shows a similar trend as shown in Figure S2. The detectivity (D^*) as a function of voltage is also show in Figure S3 and shows a similar trend to the photoresponsivity as a function of voltage (Figure S2) and to the photocurrent as a function of voltage with the highest detectivity being 20 mM GnP with $D^* = 2.03 \times 10^{11}$ cm·Hz$^{1/2}$·W^{-1} at a voltage bias of −5 V. Here, D^* is defined as $D^* = R\sqrt{\frac{A}{\overline{i_n^2}}}$, where A is the area, which for our device is 0.45 mm^2, R is the photoresponsivity, and the root-mean-squared of the noise current is $(\overline{i_n^2})^{1/2}$. The mechanism responsible for the decrease in photoresponsivity is shown in Figure 4c on the dynamic photoresponses measured on these four samples. Interestingly, the dark current for the three samples with lower GnP concentrations has comparable I_{Dark}, while the sample with 30 mM GnP concentration has a considerably increased I_{Dark}. This means that the reduced I_{ph} in the ZnO/GnP nanocomposite sample with 30 mM GnP concentration is primarily caused by the higher I_{Dark}. The rise times (fall times) are determined from the time required to go from 10 to 90% (90 to 10%) of the photocurrent and are depicted in Figure 4d. For the ZnO/GnP nanocomposite samples with for 0, 5, 20, and 30 mM GnP concentrations, the rise/fall times are 9.6 s/17.2 s, 13.5 s/10.8 s, 20.6 s/15.7 s, and 16.2 s/23.6 s, respectively. These rise and fall times and all photoresponsivity measurements were taken at a bias voltage of 5 V. Basically, the rise and fall times remain comparable at zero or low GnP concentrations. The moderately increased rise and fall times at higher GnP concentrations of 20 and 30 mM may be associated with large ZnO/GnP interfaces for charge trapping and a highly conductive percolation path through GnPs. This is caused by the GnP becoming dominant conducting materials at higher GnP concentration much like other graphene-based photoconductors, and the high conductivity of graphene can cause charges to the cycle through the material much easier and allows for a longer photoconductive decay.

The photoresponsivity as a function of the UV light power is depicted in Figure 5a. The best performance can be observed on the ZnO/GnP nanocomposite samples with a GnP concentration of 20 mM. While the sample with a GnP concentration of 30 mM suffers an increased I_{Dark}, it considerably outperforms the samples with a low GnP concentration of 5 mM and without any GnPs. The ZnO/GnP nanocomposite samples of 20 mM GnP concentration show the highest photoresponsivity of 2.2 A/W at 0.2 μW at a wavelength of 340 nm, which are 2.8 times and 4.5 times higher than those of the samples with 0 mM (0.78 A/W) and 5 mM (0.41 A/W) GnP concentrations at comparable UV light powers of 0.20 and 0.27 μW, respectively. It should be noted that the photoresponsivity decreases with increasing light power and is associated with the device reaching complete saturation of charge in the conduction band under increasing UV illumination, which means a reduction in quantum efficiency at higher intensity.[1,31] In Figure 5b, the spectral photoresponsivities (normalized to the maximum responsivity value for feasibility of comparison) for the samples with 0 and 20 mM GnP concentrations are compared. The UV−vis transmission spectra were taken on the ZnO/GnP nanocomposite samples, and the result is depicted in Figure S4. The

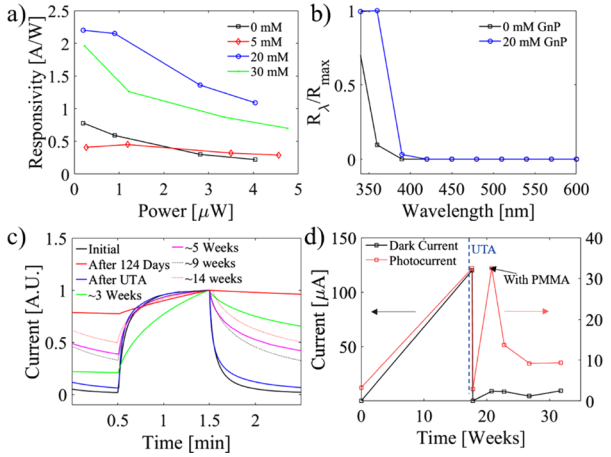

Figure 5. (a) Photoresponsivity as a function of power of the ZnO/GnP nanocomposite photodetectors with 0, 5, 20, and 30 mM GnP concentrations. Similarly, we have (b) the spectral photoresponse comparing the best result to pure ZnO, (c) dynamic photoresponse, and (d) dark current and photocurrent as a function of time before and after the UTA treatment. PMMA passivation was applied to the sample after UTA.

absorption cutoff at approximately around 380 nm is anticipated from the crystalline ZnO with a bandgap of 3.26 eV. The similar cutoffs indicate that ZnO dominates the light absorption in both samples. However, the ZnO/GnP nanocomposites induce a small red shift of 20 nm in the cutoff to 380 nm, which corresponds to the bandgap of ∼3.26 eV as opposed to ∼3.44 eV for the ZnO only sample. While the mechanism for this shift requires further investigations, we hypothesize moderate doping in ZnO through introduction of the GnPs may occur resulting in better absorption of photons as indicated in Figure S4. Nevertheless, this doping is unlikely significant as illustrated in the moderate cutoff shift and no bandgap state formation in the visible spectrum.

In Figure 5c, a series of dynamic photoreseponse curves taken on ZnO/GnP nanocomposite films of 20 mM GnPs over the course of approximately 17.7 weeks are depicted. A clear trend of elongation of rise and fall times can be observed between the solid black and red curves. This issue can be attributed to the ZnO surface contamination by air molecule attachment. To alleviate this issue, the ZnO/GnP device was treated with UTA 800 °C for 2 s.[42] Remarkably, the optoelectronic performance was resumed after the UTA as illustrated in the dynamic response comparable (blue curve) to the initial red curve. In Figure 5c, the dynamic response curves on a ZnO/GnP nanocomposite sample with PMMA printed on the top as passivation to ambient exposure are also included. The much reduced impact of the ambient exposure can be observed. To further investigate, the dark current and photocurrent are plotted as a function of time in Figure 5d where it is observed that the photocurrent and dark current increase significantly from initial fabrication to 17.7 with no passivation; however, there is severe elongation in rise and fall times as previously mentioned. After UTA indicated by the dashed vertical line in Figure 5d, it is observed that the dark current and photocurrent return to comparable values; however, a few weeks after, the photocurrent increases significantly again while maintaining a low dark current, which might be due to the PMMA slowly aging and drying over time. As time increases, the dark current more or less

DOI: 10.1021/acsomega.9b03173
ACS Omega 2019, 4, 22497−22503

Table 1. Comparison of Device Performance of Two Kinds of UV Photodetectors Based on Nanostructured Semiconductors and Graphene Nanocomposite and Semiconductors/Graphene Heterostructured Nanohybrid

device	fabrication method	device structure	rise time (s)	fall time (s)	bias (V)	wavelength (nm)	responsivity	ref
ZnO/GnP heterostructure	inkjet-printed precursor composite ink	nanocomposite	20.6	15.7	5	340	0.82 A/W	this Work
ZnO/graphene nanodot arrays	lithography/spin coating	nanocomposite	11	2.5	5	300	22.55 mA/W	30
ZnO/graphite composite	spin coating prefabricated ink	nanocomposite	2	17	1	365	1.3×10^{-4} A/W	4
Ag/graphene/ZnO	CVD/spin coating	nanohybrid	4.68	4.18	−4	320	∼0.09 A/W	29
multidimensional graphene/ZnO	hydrothermal growth/spin coating	nanohybrid	4.26	10.97	2	365	12.8 A/W	45
ZnO nanowires/graphene oxide	hydrothermal growth	nanohybrid	11.2	81	5	370	10,230 A/W	43

stays constant while the photocurrent shows an exponential decay and then begins to level off. Interestingly, the photocurrent levels off to a larger photocurrent than it had previously obtained before UTA and passivation, while also maintaining a relatively stable dark current, which indicates methods of passivation such as with PMMA that can offer a viable method for stable packaging of devices that show instability in ambient air.

Table 1 compares the device performance of the ZnO/GnP nanocomposite UV detectors in this work with a few other ZnO/graphene UV photodetectors. Basically, the photodetectors in the table can be classified into two types: nanocomposites that have advantages of low cost and scalability and heterostructured nanohybrids by stacking semiconductor photosensitizers on graphene. The UV detectors based on nanocomposites can be made by inkjet printing or other low-cost approaches from premixed ZnO/GnP inks or precursors.[4,30] Particularly, in this work, through introduction of ZnO/GnP Schottky junctions for better exciton dissociation and photocarrier transfer, high photoresponsivity up to 0.82 A/W has been obtained, which is 36 times and 6307 times better than nanocomposite UV photodetector devices ZnO/graphene nanodot arrays and ZnO/graphite nanocomposites, respectively, and 9 times better than a nanohybrid device of Ag/Graphene/ZnO photodetectors.[4,29,30] It should be noted that better device performance has been observed in nanohybrid UV detectors by optimal device design to take advantages of high carrier mobility of graphene, while scaling up the nanohybrid detectors remains challenging.[1,43−45] This means that further improvement of nanocomposite UV detectors is possible through implementing nanohybrid device designs.

CONCLUSIONS

In this work, a new ZnOPrGnP composite ink has been developed for inkjet printing ZnO/GnP bulk heterojunction nanocomposite photoconductors for ultraviolet detection. This ZnOPrGnP composite ink consists of well-dispersed GnPs of concentrations of 0, 5, 20, and 30 mM mixed with ZnOPr solution. The unique advantage of this composite ink is in optimal formation of the ZnO/GnP interface during the ZnO crystallization in the post-annealing after inkjet printing of the UV detectors. This Schottky ZnO/GnP interface plays a critical role in exciton dissociation and charge transfer as shown in the enhanced photoreponse with increasing GnP concentration in the printed ZnO/GnP bulk heterojunction nanocomposites. At an optimal GnP concentration of 20 mM, remarkable UV photoresponsivity up to 2.2 A/W has been achieved at 2.2 μW and 5 V voltage biasing, in contrast to 0.78 A/W in the samples with 0 mM GnPs measured the at similar conditions. At a higher GnP concentration of 30 mM, a noticeable increase in dark current was observed, resulting in reduction of the photoresponsivity. Finally, we have explored refreshing the the ZnO/GnP bulk heterojunction nanocomposite UV detectors using the UTA process at 800 °C for 2 s in air and confirmed that the UTA is effective in removing air molecule contamination of ZnO. Passivating the surface of the ZnO/GnP with a PMMA after UTA treatment has shown promising in prevention of the ambient degradation ZnO-based devices.

EXPERIMENTAL DETAILS

The ZnOPrGnP nanocomposite ink was obtained by mixing the GnPs into ZnO precursor solution. The ZnO sol−gel precursor solution was made following our previous works by dissolving equimolar amounts of zinc acetate dihydrate and ethanolamine (500 mL, 98%, Sigma-Aldrich) together and stirring under a heat of 60 °C until a clear gel formed. 2-Methoxyethanol was then added such that the concentration of zinc acetate dihydrate was approximately 0.3 M. The few-layer graphene nanoplatelets (GnPs) (5−8 nm thick, XGnP-M-5, XG Sciences) of 5, 20, and 30 mM concentrations were added into the ZnO sol−gel precursor solution and ultrasonicated for 1 h until evenly dispersed throughout the solution. Gold electrodes were deposited on SiO_2/Si substrates to form a 0.3 mm × 3.0 mm effective printing area using e-beam evaporation of Au (40 nm)/Ti (5 nm) with a shadow mask. The substrate was heated with a hot plate to a temperature of 50 °C before printing. The ink was then dispensed utilizing a piezoelectric vibration with the nozzle placed at a distance of ∼20 μm from the surface so that a capillary attraction of the liquid to the substrate forms for easy dispensing. The printed area of the ink is approximately 0.40 ± 0.1 mm^2 and was cured at 180 °C for 10 min after printing. The inkjet printer used is a SonoPlot Microplotter Proto (Sonoplot) operated with SonoGuide and SonoDraw software. The inkjet printer tips are boron silica glass pipettes stretched out using a laser puller (P-2000 Micropipette Puller System, Sutter Instrument Company), and the nozzle diameters are roughly ∼150 μm. Once the curing of the printed ink was completed, the samples were placed into a furnace set to ramp up at a rate of 5 °C/min to a temperature of 350 °C for 2 h in air followed with cooling with furnace power off. After samples were cooled down, their optoelectronic performance was characterized immediately. Since ZnO nanostructures have a large surface area that can be post-contaminated in air and degraded performance afterward,

DOI: 10.1021/acsomega.9b03173
ACS Omega 2019, 4, 22497−22503

some samples of long air exposure were treated with the ultrafast thermal annealing (UTA) that turned out to be efficient to remove the surface contamination as illustrated in the comparable optoelectronic performance to that of freshly fabricated ZnO/GnP bulk heterojunction devices.[42] Optical images and scanning electron microscopy (SEM, JEOL JSM-6380) images were taken to reveal the sample morphology and uniformity. Raman spectra and maps (Alpha 300 Confocal Raman, WiTec) were collected to analyze the sample phase and crystallinity and the distribution of GnPs in the printed GnP/ZnO films. Photoresponse measurements were performed using a CHI660D electrochemical workstation with a Newport Oriel Apex monochromator and Oriel Cornerstone 140 1/8m monochromator filter in the UV−visible spectra.

■ ASSOCIATED CONTENT

Supporting Information

The Supporting Information is available free of charge at https://pubs.acs.org/doi/10.1021/acsomega.9b03173.

Contents include Raman and optical transmission spectra and photoresponsivity and detectivity as a function of bias voltages across the devices (PDF)

■ AUTHOR INFORMATION

Corresponding Authors

*E-mail: bkcook@ku.edu (B.C.).
*E-mail: jwu@ku.edu (J.W.).

ORCID

Brent Cook: 0000-0001-9288-7267

Notes

The authors declare no competing financial interest.

The Kansas City National Security Campus is operated by Honeywell Federal Manufacturing & Technologies, LLC for the United States Department of Energy under contract no. DE-NA0002839.

■ ACKNOWLEDGMENTS

This research was supported by Plant Directed Research and Development funds from the Department of Energy's Kansas City National Security Campus, operated and managed by Honeywell Federal Manufacturing and Technologies, LLC under contract no. DE-NA0002839. The authors also acknowledge support in part by ARO contract no. W911NF-16-1-0029 and NSF contracts nos. NSF-DMR-1508494, NSF-DMR-1909292, and NSF-ECCS-1809293.

■ REFERENCES

(1) Gong, M.; Liu, Q.; Cook, B.; Kattel, B.; Wang, T.; Chan, W. L.; Ewing, D.; Casper, M.; Stramel, A.; Wu, J. Z. All-Printable ZnO Quantum Dots/Graphene van der Waals Heterostructures for Ultrasensitive Detection of Ultraviolet Light. *ACS Nano* **2017**, *11*, 4114−4123.

(2) Guo, W.; Xu, S.; Wu, Z.; Wang, N.; Loy, M. M. T.; Du, S. Oxygen-assisted charge transfer between ZnO quantum dots and graphene. *Small* **2013**, *9*, 3031−3036.

(3) Liu, Q.; Gong, M.; Cook, B.; Ewing, D.; Casper, M.; Stramel, A.; Wu, J. Transfer-free and printable graphene/ZnO-nanoparticle nanohybrid photodetectors with high performance. *J. Mater. Chem. C* **2017**, *5*, 6427−6432.

(4) Padmanabhan, M.; Meyen, R.; Houghton, K. Facile fabrication of ZnO—graphite composite thin films for ultraviolet photodetection. *Mater. Res. Express* **2018**, *5*, No. 095606.

(5) Cook, B.; Liu, Q.; Gong, M.; Ewing, D.; Casper, M.; Stramel, A.; Wu, J. Quantum Dots-Facilitated Printing of ZnO Nanostructure Photodetectors with Improved Performance. *ACS Appl. Mater. Interfaces* **2017**, *9*, 23189−23194.

(6) Kim, S.; Choi, Y. J.; Choi, Y.; Kang, M. S.; Cho, J. H. Large-Area Schottky Barrier Transistors Based on Vertically Stacked Graphene-Metal Oxide Heterostructures. *Adv. Funct. Mater.* **2017**, *27*, 1700651.

(7) Monreal-Bernal, A.; Vilatela, J. J. Large-Area Schottky Junctions between ZnO and Carbon Nanotube Fibres. *ChemPlusChem* **2018**, *83*, 285−293.

(8) Nie, B.; Hu, J. G.; Luo, L. B.; Xie, C.; Zeng, L. H.; Lv, P.; Li, F. Z.; Jie, J. S.; Feng, M.; Wu, C. Y.; Yu, Y. Q.; Yu, S. H. Monolayer graphene film on ZnO nanorod array for high-performance Schottky junction ultraviolet photodetectors. *Small* **2013**, *9*, 2872−2879.

(9) Yatskiv, R.; Grym, J. Temperature-dependent properties of semimetal graphite-ZnO Schottky diodes. *Appl. Phys. Lett.* **2012**, *101*, 162106.

(10) Zhu, Z.; Wang, S.; Zhu, Y.; Liu, X.; Zou, Y.; Gu, Y.; Ju, D.; Zeng, H. Fiber-Shaped ZnO/Graphene Schottky Photodetector with Strain Effect. *Adv. Mater. Interfaces* **2018**, *5*, 1800136.

(11) Ning, Y.; Zhang, Z.; Teng, F.; Fang, X. Novel Transparent and Self-Powered UV Photodetector Based on Crossed ZnO Nanofiber Array Homojunction. *Small* **2018**, *14*, 1703754.

(12) Lee, H.-Y.; Heish, Y.-C.; Lee, C.-T. High sensitivity detection of nitrogen oxide gas at room temperature using zinc oxide-reduced graphene oxide sensing membrane. *J. Alloys Compd.* **2019**, *773*, 950−954.

(13) Yatskiv, R.; Grym, J.; Gladkov, P.; Cernohorsky, O.; Vanis, J.; Maixner, J.; Dickerson, J. H. Room temperature hydrogen sensing with the graphite/ZnO nanorod junctions decorated with Pt nanoparticles. *Solid-State Electron.* **2016**, *116*, 124−129.

(14) Chen, Z.; Wang, Z.; Li, X.; Lin, Y.; Luo, N.; Long, M.; Zhao, N.; Xu, J. B. Flexible Piezoelectric-Induced Pressure Sensors for Static Measurements Based on Nanowires/Graphene Heterostructures. *ACS Nano* **2017**, *11*, 4507−4513.

(15) Shin, S. H.; Park, D. H.; Jung, J. Y.; Lee, M. H.; Nah, J. Ferroelectric Zinc Oxide Nanowire Embedded Flexible Sensor for Motion and Temperature Sensing. *ACS Appl. Mater. Interfaces* **2017**, *9*, 9233−9238.

(16) Gao, N.; Fang, X. Synthesis and Development of Graphene-Inorganic Semiconductor Nanocomposites. *Chem. Rev.* **2015**, *115*, 8294−8343.

(17) Castro Neto, A. H.; Guinea, F.; Peres, N. M. R.; Novoselov, K. S.; Geim, A. K. The electronic properties of graphene. *Rev. Mod. Phys.* **2009**, *81*, 109−162.

(18) Janotti, A.; Van de Walle, C. G. Fundamentals of zinc oxide as a semiconductor. *Rep. Prog. Phys.* **2009**, *72*, 126501.

(19) Liang, F.-X.; Gao, Y.; Xie, C.; Tong, X.-W.; Li, Z.-J.; Luo, L.-B. Recent advances in the fabrication of graphene−ZnO heterojunctions for optoelectronic device applications. *J. Mater. Chem. C* **2018**, *6*, 3815−3833.

(20) Azhar, E. A.; Vanjaria, J.; Ahn, S.; Fou, T.; Dey, S. K.; Salagaj, T.; Sbrockey, N.; Tompa, G. S.; Yu, H. Vapor-Transport Synthesis and Annealing Study of $Zn_xMg_{1-x}O$ Nanowire Arrays for Selective, Solar-Blind UV-C Detection. *ACS Omega* **2018**, *3*, 4899−4907.

(21) Cook, B.; Liu, Q.; Liu, J.; Gong, M.; Ewing, D.; Casper, M.; Stramel, A.; Wu, J. Facile zinc oxide nanowire growth on graphene via a hydrothermal floating method: towards Debye length radius nanowires for ultraviolet photodetection. *J. Mater. Chem. C* **2017**, *5*, 10087−10093.

(22) Liu, J.; Lu, R.; Xu, G.; Wu, J.; Thapa, P.; Moore, D. Development of a Seedless Floating Growth Process in Solution for Synthesis of Crystalline ZnO Micro/Nanowire Arrays on Graphene: Towards High-Performance Nanohybrid Ultraviolet Photodetectors. *Adv. Funct. Mater.* **2013**, *23*, 4941−4948.

(23) Liu, R.; Peng, M.; Zhang, H.; Wan, X.; Shen, M. Atomic layer deposition of ZnO on graphene for thin film transistor. *Mater. Sci. Semicond. Process.* **2016**, *56*, 324−328.

DOI: 10.1021/acsomega.9b03173
ACS Omega 2019, 4, 22497−22503

(24) Maurya, M. R.; Toutam, V.; Haranath, D. Comparative Study of Photoresponse from Vertically Grown ZnO Nanorod and Nanoflake Films. *ACS Omega* **2017**, *2*, 5538−5544.
(25) Tran, V. T.; Wei, Y.; Yang, H.; Zhan, Z.; Du, H. All-inkjet-printed flexible ZnO micro photodetector for a wearable UV monitoring device. *Nanotechnology* **2017**, *28*, No. 095204.
(26) Hassan, G.; Bae, J.; Hassan, A.; Ali, S.; Lee, C. H.; Choi, Y. Inkjet printed stretchable strain sensor based on graphene/ZnO composite on micro-random ridged PDMS substrate. *Composites, Part A* **2018**, *107*, 519−528.
(27) Dong, Y.; Zou, Y.; Song, J.; Li, J.; Han, B.; Shan, Q.; Xu, L.; Xue, J.; Zeng, H. An all-inkjet-printed flexible UV photodetector. *Nanoscale* **2017**, *9*, 8580−8585.
(28) Gupta, A. A.; Arunachalam, S.; Cloutier, S. G.; Izquierdo, R. Fully Aerosol-Jet Printed, High-Performance Nanoporous ZnO Ultraviolet Photodetectors. *ACS Photonics* **2018**, *5*, 3923−3929.
(29) Ju, D.; Liu, X.; Zhu, Z.; Wang, S.; Liu, S.; Gu, Y.; Chang, J.; Liu, Q.; Zou, Y. Solution processed membrane-based wearable ZnO/graphene Schottky UV photodetectors with imaging application. *Nanotechnology* **2019**, *30*, 375701.
(30) Tang, R.; Han, S.; Teng, F.; Hu, K.; Zhang, Z.; Hu, M.; Fang, X. Size-Controlled Graphene Nanodot Arrays/ZnO Hybrids for High-Performance UV Photodetectors. *Adv. Sci.* **2018**, *5*, 1700334.
(31) Cook, B.; Liu, Q.; Butler, J.; Smith, K.; Shi, K.; Ewing, D.; Casper, M.; Stramel, A.; Elliot, A.; Wu, J. Heat-Assisted Inkjet Printing of Tungsten Oxide for High-Performance Ultraviolet Photodetectors. *ACS Appl. Mater. Interfaces* **2018**, *10*, 873−879.
(32) Cook, B.; Liu, Q.; Gong, M.; Ewing, D.; Casper, M.; Stramel, A.; Elliot, A.; Wu, J. Printing High-Performance Tungsten Oxide Thin Film Ultraviolet Photodetectors on ZnO Quantum Dot Textured SiO_2 Surface. *IEEE Sens. J.* **2018**, *18*, 9542−9547.
(33) Begines, B.; Hook, A. L.; Alexander, M. R.; Tuck, C. J.; Wildman, R. D. Development, printability and post-curing studies of formulations of materials resistant to microbial attachment for use in inkjet based 3D printing. *Rapid Prototyping J.* **2016**, *22*, 835−841.
(34) Gao, M.; Li, L.; Song, Y. Inkjet printing wearable electronic devices. *J. Mater. Chem. C* **2017**, *5*, 2971−2993.
(35) Zhang, T.-F.; Wu, G.-A.; Wang, J.-Z.; Yu, Y.-Q.; Zhang, D.-Y.; Wang, D.-D.; Jiang, J.-B.; Wang, J.-M.; Luo, L.-B. A sensitive ultraviolet light photodiode based on graphene-on-zinc oxide Schottky junction. *Nanophotonics* **2017**, *6*, 1073−1081.
(36) Di Bartolomeo, A. Graphene Schottky diodes: An experimental review of the rectifying graphene/semiconductor heterojunction. *Phys. Rep.* **2016**, *606*, 1−58.
(37) Ponosov, Y. S.; Ushakov, A. V.; Streltsov, S. V. Electronic Raman scattering in graphite and single-layer and few-layer graphene. *Phys. Rev. B* **2015**, *91*, 195435.
(38) Bokobza, L.; Bruneel, J.-L.; Couzi, M. Raman Spectra of Carbon-Based Materials (from Graphite to Carbon Black) and of Some Silicone Composites. *J. Carbon Res. C* **2015**, 77−94.
(39) Pramanik, A.; Biswas, S.; Tiwary, C. S.; Sarkar, R.; Kumbhakar, P. Colloidal N-Doped Graphene Quantum Dots with Tailored Luminescent Downshifting and Detection of UVA Radiation with Enhanced Responsivity. *ACS Omega* **2018**, *3*, 16260−16270.
(40) Huanga, Y.; Liu, M.; Li, Z.; Zeng, Y.; Liu, S. Raman spectroscopy study of ZnO-based ceramic films fabricated by novel sol-gel process. *Mater. Sci. Eng., B* **2003**, *97*, 111−116.
(41) Lin, C. H.; Cheng, B.; Li, T. Y.; Retamal, J. R. D.; Wei, T. C.; Fu, H. C.; Fang, X.; He, J. H. Orthogonal Lithography for Halide Perovskite Optoelectronic Nanodevices. *ACS Nano* **2019**, *13*, 1168−1176.
(42) Liu, Q.; Gong, M.; Cook, B.; Ewing, D.; Casper, M.; Stramel, A.; Wu, J. Fused Nanojunctions of Electron-Depleted ZnO Nanoparticles for Extraordinary Performance in Ultraviolet Detection. *Adv. Mater. Interfaces* **2017**, *4*, 1601064.
(43) AlZoubi, T.; Qutaish, H.; Al-Shawwa, E.; Hamzawy, S. Enhanced UV-light detection based on ZnO nanowires/graphene oxide hybrid using cost-effective low temperature hydrothermal process. *Opt. Mater.* **2018**, *77*, 226−232.
(44) Gong, M.; Sakidja, R.; Goul, R.; Ewing, D.; Casper, M.; Stramel, A.; Elliot, A.; Wu, J. Z. High-Performance All-Inorganic $CsPbCl_3$ Perovskite Nanocrystal Photodetectors with Superior Stability. *ACS Nano* **2019**, *13*, 1772−1783.
(45) Ko, K. B.; Ryu, B. D.; Han, M.; Hong, C.-H.; Dinh, D. A.; Cuong, T. V. Multidimensional graphene and ZnO-based heterostructure for flexible transparent ultraviolet photodetector. *Appl. Surf. Sci.* **2019**, *481*, 524−530.

DOI: 10.1021/acsomega.9b03173
ACS Omega 2019, 4, 22497−22503